OPEN ACCESS
IOP Publishing
Journal of Physics G: Nuclear and Particle Physics
J. Phys. G: Nucl. Part. Phys. **47** (2020) 045111 (17pp)
https://doi.org/10.1088/1361-6471/ab67e6

Transverse momentum spectra of J/ψ produced in collisions over an energy range from 17.4 GeV to 13 TeV

Ya-Hui Chen[1,2], Yu-Gang Ma[3,2], Guo-Liang Ma[3,2] and Jin-Hui Chen[3,2]

[1] Department of Physics, College of Basic Medical Sciences, Army Medical University, Chongqing 400038, People's Republic of China
[2] Shanghai Institute of Applied Physics, Chinese Academy of Sciences, Shanghai 201800, People's Republic of China
[3] Key Laboratory of Nuclear Physics and Ion-beam Application (MOE), Institute of Modern Physics, Fudan University, Shanghai 200433, People's Republic of China

E-mail: yahuierdongchen@163.com, mayugang@fudan.edu.cn, glma@fudan.edu.cn and jhchen@rcf.rhic.bnl.gov

Received 21 April 2019, revised 29 December 2019
Accepted for publication 6 January 2020
Published 5 March 2020

Abstract

Transverse momentum spectra of inclusive J/ψ mesons produced in particle–particle, particle–nucleus and nucleus–nucleus collisions over a center-of-mass energy range from 17.4 GeV to 13 TeV are analyzed by a multi-component Schwinger mechanism. The model results are found to fit the experimental data measured by the ALICE, CDF, D0, HERA-B, E789, NA50, E705, LHCb and PHENIX Collaborations. We extract the distribution of minimum distance between the partons which form the charmonium $c\bar{c}$. Moreover, the energy and rapidity dependent free parameters in Schwinger mechanism are obtained. The parameter related to string tension is found to increase with the increase of energy and to decrease with the increase of rapidity and centrality.

Keywords: transverse momentum spectra, Schwinger mechanism, minimum distance, high energy collisions

(Some figures may appear in colour only in the online journal)

1. Introduction

In order to explore the evolution of the Universe and the origin of matter, scientists in nuclear and particle fields build high energy heavy ion colliders to look for the quark-gluon plasma (QGP) [1] and study its properties in high energy collisions. In theory, QGP is a kind of approximately perfect fluid and color-deconfined about the strong interactions, with an energy density far in excess of 1 GeV fm^{-3}. This matter may be produced in nuclear collisions at the Relativistic Heavy Ion Collider (RHIC) [2–7] and Large Hadron Collider (LHC) [8, 9]. It also be very likely to exist in the first few microseconds of the early universe and the interior of neutron stars. Therefore, it is very meaningful to study its nature. However, its existence under extremely high temperature and energy density conditions in a very short time makes it impossible to be measured directly in experiments. Thus, researchers often analyze the final state particles spectra at (chemical and kinetic) freeze-out to extract the thermodynamic characteristics of interacting system through different theoretical models and give some predictions on the new behaviors [10–14].

Since the middle of last century, nuclear physics has developed rapidly. Some large experimental facilities, such as accelerators and detectors, have been set up one after another. A series of experiments have been done by different collaborations at the Tevatron Collider in the High Intensity Laboratory (HIL) of the Fermi National Accelerator Laboratory (FNAL), the Hadron-Electron Ring Accelerator (HERA) in the German Electron Synchrotron Laboratory (DESY), the RHIC in the Brookhaven National Laboratory (BNL), as well as the Super Proton Synchrotron (SPS) and LHC at European Laboratory for Particle Physics (CERN), respectively. A large number of experimental data provide convenience for the theorists to do research in detail.

Among the experimental observations, the transverse momentum spectra of final state particles play a very significant role, which reflect the transverse excitation degree of interaction system. In high energy collisions, heavy quarks, produced in hard partonic scatterings of the initial stages, experience the whole evolution of the QGP and will be preserved throughout the subsequent thermal evolution. Therefore, they can be used as probes for characterising the QGP medium [15]. While traveling in the QGP, the heavy quarks will lose some of their energies [16], which may be reflected in the distribution of transverse momentum. The charmonium is a bound quarkonia state of $c\bar{c}$ pair at the hadronization stage, and its production is also a meaningful interest in the heavy flavor topics [17, 18]. In this work, we focus our attention on the production of charmonium.

Many kinds of theoretical models are proposed to explain the behaviors of the final state particles produced in high energy collisions. These models include, but do not limited to, the statistical hadronization model [19], kinetic formation model [20, 21], quark model [22], multi-source model [23, 24], and so forth. More early, in order to examine the production of electron-positron pair in a strong and uniform electric field, the Schwinger mechanism of pair production was firstly put forth [25, 26], and has been applied to study the particle production in Quantum Chromodynamics (QCD) [27–29]. The pair production of charm quarks is one of the most attractive topics for studying strong interactions. The charmonium J/ψ production in heavy-ion collisions has been contributed from both initial production [30], color screening [31], continuous regeneration [32]. In the present work, based on the multisource model, we adopt the Schwinger mechanism to describe the transverse momentum spectra of J/ψ produced in particle–particle, particle–nucleus and nucleus–nucleus collisions in the center-of-mass energy range from 17.4 GeV to 13 TeV, which involve the above production mechanisms in principle. The distributions of minimum distance between the partons which form the charmonium ($c\bar{c}$) can be extracted. We find that the behaviors of some parameters depending on the center-of-mass energy, centrality bin, rapidity and momentum, which would provide some useful information about the production mechanisms of J/ψ.

This paper is structured as follows. First, we describe the model and method in section 2. Results and discussion are presented in section 3. Finally, we summarize our main observations and conclusions.

2. The model and method

Heavy ion collisions can be described by color strings stretched between the projectile and target nucleons, which will decay into new strings through the production of quark-antiquark pairs ($q\bar{q}$) and subsequently form the observable hadrons [33]. Furthermore, the production of $q\bar{q}$ pairs can be analyzed by the Schwinger mechanism [25, 26].

In quantum electrodynamics (QED), the particle production rate of Schwinger electron-positron pairs satisfies the following function

$$f(m) \sim \exp(-\pi m^2/eE),$$

where E is the electric field strength. From the results in QED, it is easy to obtain the results in QCD. In QCD, the tunneling probability of the primarily partons with m_t is given by the following form

$$\mathrm{d}n/\mathrm{d}^2p_T \sim \exp(-\pi m_t^2/\kappa),$$

where κ denotes the tension of strings (energy per unit length of the string, GeV fm^{-1}) [34], which are usually formed due to the existence of strong interactions between partons, m_0 and $m_t = \sqrt{p_t^2 + m_0^2}$, which respectively denote the rest and transverse mass of partons. Corresponding to charm quarks, the value of m_0 used in the present work is 1.275 GeV.

During the high energy collisions, with the expansion of interaction system, the energy density and temperature will reduce, and the formation of strings is impossible in a certain equilibrium state. For simplicity, we divide the continuous processes into several relatively independent stages of a quasi-equilibrium process. Every stage can be regarded as an independent component to produce the strings in an equilibrium state, then the string tension will be the average result of all the strings in one component.

In the framework of multisource model [23], considering the simplest fluctuation of the string tension around its mean value with the normal distribution, the probability distribution of transverse momentum for the partons from the jth component can be rewritten as [35]

$$\begin{aligned} f_j(p_t) &= C_0(\kappa_j)\exp\left(-\frac{\pi(p_t^2 + m_0^2)}{\kappa_j}\right) \\ &= \frac{2}{\sqrt{\kappa_j}}\exp\left(-\frac{\pi p_t^2}{\kappa_j}\right), \end{aligned} \tag{1}$$

where C_0 is the normalization constant which can be calculated in the following way,

$$\begin{aligned} C_0(\kappa_j) &= \frac{1}{\int_0^\infty \exp(-\pi(p_t^2 + m_0^2)/\kappa_j)\mathrm{d}p_t} \\ &= \frac{2}{\sqrt{\kappa_j}}\exp\left(\frac{\pi m_0^2}{\kappa_j}\right). \end{aligned} \tag{2}$$

We assume that the basic impacting process in high energy collisions is the binary parton–parton interaction, and the final state particles can be regarded as the fusion results of partons. Then the energy of a bound state, $q\bar{q}$, will be the sum energy of the two partons and

can be expressed with the string tension. Considering the situation that the transverse momentum of the two partons are in the same direction, then the probability distribution of transverse momentum (p_T) of final state particles contributed by two partons from the jth component can be written as the folding of equation (1),

$$\begin{aligned} f_j(p_T) &= \int_0^{p_T} f_{j1}(p_t)\cdot f_{j2}(p_T - p_t)\mathrm{d}p_t \\ &= \frac{4}{\kappa_j}\int_0^{p_T}\exp\left(-\frac{\pi(p_t^2 + (p_T - p_t)^2)}{\kappa_j}\right)\mathrm{d}p_t \\ &= \frac{2\sqrt{2}}{\sqrt{\kappa_j}}\exp\left(-\frac{\pi}{2\kappa_j}p_T^2\right)Erf_j\left(\sqrt{\frac{\pi}{2\kappa_j}}p_T\right), \end{aligned} \tag{3}$$

where,

$$Erf(x) = \frac{2}{\sqrt{\pi}}\int_0^x \exp(-t^2)\mathrm{d}t. \tag{4}$$

and the normalization constant is $\frac{2\sqrt{2}}{\sqrt{\kappa_j}}$.

Further, considering the $q\bar{q}$ produced in the collisions, such as $c\bar{c}$ studied in the present work, we can extract the minimum distance between the two partons (which will form the observable particles subsequently). Generally, the primary strings created by the partons stay at an excited state and can be viewed as small discs in the transverse space. With the increases of the collision energy, the number of the partons increase and the strings begin to overlap. Simultaneously, the strings may fuse stochastically to form particles. Sometimes, one particle may be the fusion result of several strings. If we consider the partons which form the strings and subsequently fuse to produce observable particles to be independent, the minimum distance between the partons which form the identified particles in the jth component can be expressed in the form of [36]

$$L_j = \frac{2m_T}{\kappa_j} = \frac{2\sqrt{p_T^2 + m_0^2}}{\kappa_j}. \tag{5}$$

Combining equations (3)–(5), we can get the probability distribution of the minimum distance between partons which form the identified particles in the jth component through the following formula,

$$\begin{aligned} f_j(L) &= f_j(p_T)\cdot\frac{\kappa_j}{2p_T}\cdot\sqrt{p_T^2 + m_0^2} \\ &= \frac{L\kappa_j}{p_T}\int_0^{p_T}\exp\left(-\frac{\pi}{\kappa_j}(p_t^2 + (p_T - p_t)^2)\right)\mathrm{d}p_t \\ &= \frac{\sqrt{2}L\kappa_j^{3/2}}{\sqrt{\kappa_j^2L^2 - 4m_0^2}}\exp\left(-\frac{\pi(\kappa_j^2L^2 - 4m_0^2)}{8\kappa_j}\right) \\ &\quad\cdot Erf_j\left(\frac{1}{2}\sqrt{\frac{\pi(\kappa_j^2L^2 - 4m_0^2)}{2\kappa_j}}\right). \end{aligned} \tag{6}$$

Note that the integral of $f_j(L)$ is also normalized to unity. Based on the probability distribution of transverse momentum and the minimum distance between partons in the jth component (equations (3) and (6)), we can get access to the averaged (squared) transverse momentum of

final state particles from the *j*th component,

$$\langle p_{T_j} \rangle = \int_0^\infty f_j(p_T) \cdot p_T \, \mathrm{d}p_T = \frac{2\sqrt{\kappa_j}}{\pi}, \tag{7}$$

$$\langle p_{T_j}^2 \rangle = \int_0^\infty f_j(p_T) \cdot p_T^2 \, \mathrm{d}p_T = \frac{(\pi + 2)\kappa_j}{\pi^2}. \tag{8}$$

For the massless particles, we can have the averaged (squared) minimum distance of final state particles from the *j*th component,

$$\langle L_j \rangle = \int_0^\infty f_j(L) \cdot L \mathrm{d}L = \frac{4}{\pi\sqrt{\kappa_j}}, \tag{9}$$

$$\langle L_j^2 \rangle = \int_0^\infty f_j(L) \cdot L^2 \mathrm{d}L = \frac{4(\pi + 2)}{\pi^2 \kappa_j}. \tag{10}$$

Considering all the components in the multisource model [23], we can get the final form of transverse momentum and minimum distance distribution as followings

$$f(p_T) = \sum_{j=1}^{M} k_j \cdot f_j(p_T), \tag{11}$$

$$f(L) = \sum_{j=1}^{M} k_j \cdot f_j(L), \tag{12}$$

where k_j is the relative ratio corresponding to the *j*th component and the integrals of $f(p_T)$ and $f(L)$ are also normalized to unity. $f_j(p_T)$ and $f_j(L)$ are given by equations (3) and (6), respectively. Note that $f_j(p_T)$ (or $f_j(L)$) from different sources are in a same form but with different string tension parameters κ_j. We will give an empirical relation for different sources of string tension parameters in which all κ_j are related to κ_0 in the next section. Therefore, the free parameters are κ_0 and k_j in our model. In our model, the total number of components $M = 2$, 3, or 4, which depends on the available p_T range of experimental data.

Thus, we can use the string tension and the minimum distance between partons which form the identified particles to describe the corresponding energy of partons and the violent degree of collisions, respectively. The strength in the strings are stronger, the string tension are larger, the corresponding energies of partons are higher, the minimum distance between partons are smaller, and the collisions are more violent.

3. Results and discussion

Figures 1(a)–(c) present the double-differential spectra, $\mathrm{d}^2\sigma/(\mathrm{d}y\mathrm{d}p_T)$, of the inclusive J/ψ mesons produced in proton–proton (pp) and proton-anti-proton ($p\overline{p}$) collisions at high energies for the dimuon ($\mu^+\mu^-$) decay channels, where σ on the vertical axis denote the cross-section. The corresponding rapidity intervals, collision energies and integrated luminosities are marked in the panels. In figure 1(a), we use different powers of ten marked in the panel to scale the data measured at different collision energies for clarity. The different symbols in panels 1(a)–(c) denote the experimental data measured by the (a) ALICE Collaboration [37, 38] at CERN LHC, (b) CDF Collaboration [39, 40] and (c) D0 Collaboration [41] in the FNAL. The vertical error bars given by the ALICE Collaboration present the total uncertainties which combine the systematic and statistical uncertainties by their root-sum-square,

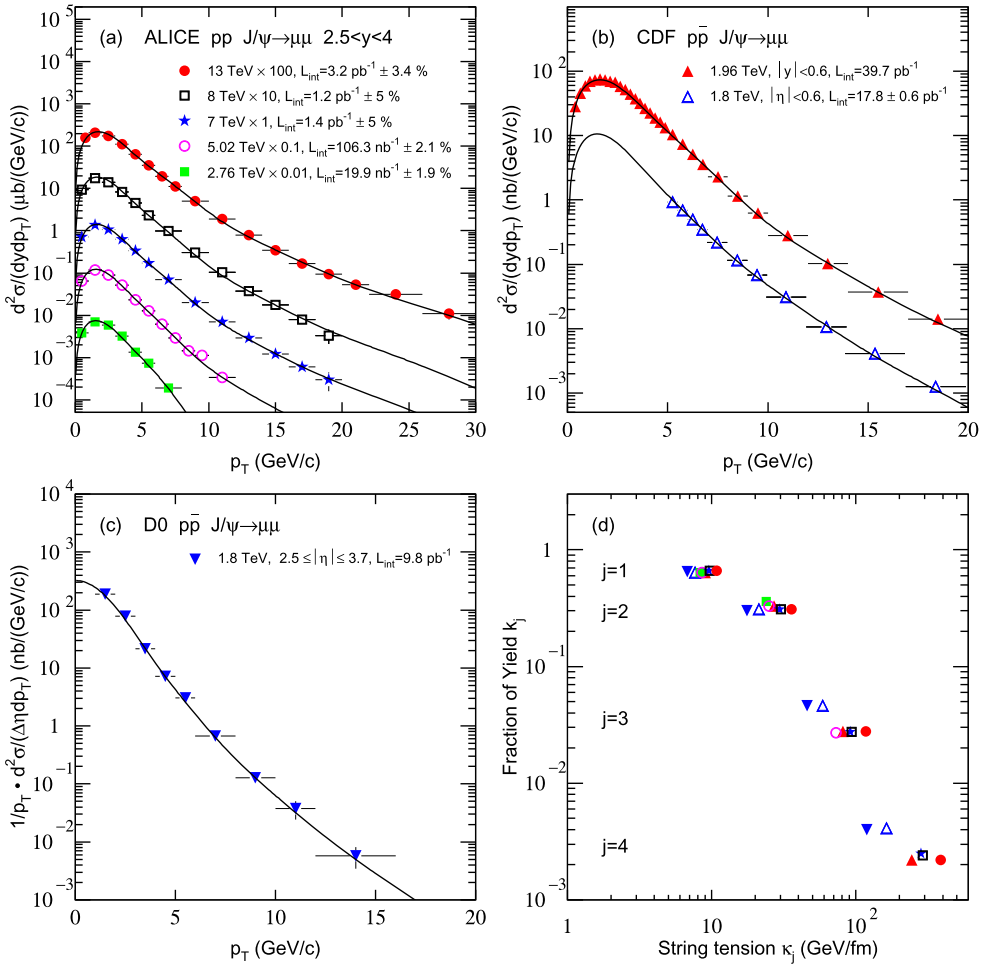

Figure 1. (a)–(c) Transverse momentum spectra of inclusive J/ψ mesons produced in collisions at TeV, where the collision types, decay modes, rapidity intervals and the center-of-mass energies are marked in the panels. The different symbols represent the experimental data measured by the ALICE [37, 38], CDF [39, 40] and D0 [41] Collaborations. The different symbols in panels (a)–(c) present the experimental data, and the solid curves are the model results of the multi-component Schwinger mechanism. The data at different energies in panel (a) are scaled down by different powers of ten for clarity. (d) The relative contribution of different components corresponding to the curves in panels (a)–(c).

while the vertical error bars given by the CDF and D0 Collaborations only represent the statistical uncertainties. In some cases, the error bars are smaller than the symbols. The solid curves are fitted by equations (3) and (11), which are the results of the multi-component Schwinger mechanism. The value of free parameters (κ_0 and k_j) corresponding to the curves in figures 1(a)–(c) are listed in table 1. Figure 1(d) presents the relative ratio for different components corresponding to the curves in figures 1(a)–(c). One can see that the $\mathrm{d}^2\sigma/(\mathrm{d}y\mathrm{d}p_T)$ spectra in the transverse momentum domain $0 < p_T < 30$ GeV c^{-1} in pp or $p\overline{p}$ collisions at TeV energies are fitted well.

Table 1. Values of free parameters (κ_0, k_1, k_2, k_3, and k_4) for the curves in figures 1–3.

Figures	Collaboration	Type	(Pseudo)rapidity	$\sqrt{s_{\rm NN}}$ (GeV)	κ_0	k_1	k_2	k_3	k_4	χ^2/ndf
Figure 1(a)	ALICE	pp	$\mu\mu$, $2.5 < y < 4$	13000	3.29 ± 0.16	0.66 ± 0.03	0.31 ± 0.03	0.0278 ± 0.0150	0.0022 ± 0.0022	0.923
Figure 1(a)	ALICE	pp	$\mu\mu$, $2.5 < y < 4$	8000	3.11 ± 0.15	0.66 ± 0.03	0.31 ± 0.03	0.0276 ± 0.0150	0.0024 ± 0.0024	0.691
Figure 1(a)	ALICE	pp	$\mu\mu$, $2.5 < y < 4$	7000	3.09 ± 0.15	0.66 ± 0.03	0.31 ± 0.03	0.0275 ± 0.0150	0.0025 ± 0.0025	0.419
Figure 1(a)	ALICE	pp	$\mu\mu$, $2.5 < y < 4$	5020	2.92 ± 0.15	0.64 ± 0.03	0.33 ± 0.03	0.0270 ± 0.015	0.0030 ± 0.0030	0.943
Figure 1(a)	ALICE	pp	$\mu\mu$, $2.5 < y < 4$	2760	2.88 ± 0.14	0.64 ± 0.03	0.36 ± 0.03	—	—	0.294
Figure 1(b)	CDF	$p\bar{p}$	$\mu\mu$, $\lvert y\rvert < 0.6$	1960	3.00 ± 0.15	0.64 ± 0.03	0.33 ± 0.03	0.0278 ± 0.0150	0.0022 ± 0.0022	3.857
Figure 1(b)	CDF	$p\bar{p}$	$\mu\mu$, $\lvert\eta\rvert < 0.6$	1800	2.77 ± 0.14	0.64 ± 0.03	0.31 ± 0.03	0.0460 ± 0.0230	0.0040 ± 0.0040	0.341
Figure 1(c)	D0	$p\bar{p}$	$\mu\mu$, $2.5 \leqslant \lvert\eta\rvert \leqslant 3.7$	1800	2.60 ± 0.13	0.65 ± 0.03	0.30 ± 0.03	0.046 ± 0.023	0.004 ± 0.004	6.285
Figure 2(a)	HERA-B	p-C	$\mu\mu + ee$, $\lvert y\rvert \leqslant 1.185 \sim 1.345$	41.6	1.71 ± 0.09	0.60 ± 0.03	0.30 ± 0.03	0.100 ± 0.050	—	0.842
Figure 2(a)	HERA-B	p-Ti	$\mu\mu + ee$, $\lvert y\rvert \leqslant 1.185 \sim 1.345$	41.6	1.79 ± 0.09	0.66 ± 0.03	0.30 ± 0.03	0.040 ± 0.020	—	0.427
Figure 2(a)	HERA-B	p-W	$\mu\mu + ee$, $\lvert y\rvert \leqslant 1.185 \sim 1.345$	41.6	1.79 ± 0.09	0.53 ± 0.03	0.42 ± 0.03	0.050 ± 0.030	—	0.975
Figure 2(b)	E789	p-Au	$\mu\mu$, $\lvert y\rvert \leqslant 0.425$	38.8	1.75 ± 0.09	0.64 ± 0.03	0.31 ± 0.03	0.050 ± 0.030	—	0.927
Figure 2(b)	NA50	Pb–Pb, Cent.	$\mu\mu$, $0 \leqslant y \leqslant 1$	17.4	1.61 ± 0.08	0.69 ± 0.03	0.31 ± 0.03	—	—	4.539
Figure 2(c)	E705	π^--Li	$\mu\mu$, $\lvert\eta\rvert \leqslant 1.040$	23.7	1.51 ± 0.08	0.64 ± 0.03	0.30 ± 0.03	0.060 ± 0.030	—	1.983
Figure 2(c)	E705	π^+-Li	$\mu\mu$, $\lvert\eta\rvert \leqslant 1.040$	23.7	1.49 ± 0.07	0.64 ± 0.03	0.30 ± 0.03	0.060 ± 0.030	—	1.194
Figure 2(c)	E705	p-Li	$\mu\mu$, $\lvert\eta\rvert \leqslant 2.008$	23.8	1.46 ± 0.07	0.64 ± 0.03	0.31 ± 0.03	0.050 ± 0.030	—	1.042
Figure 2(c)	E705	$\bar{p}$-Li	$\mu\mu$, $\lvert\eta\rvert \leqslant 2.008$	23.8	1.54 ± 0.08	0.64 ± 0.03	0.31 ± 0.03	0.050 ± 0.030	—	0.212
Figure 3(a)	LHCb	pp	$\mu\mu$, $2.0 < y < 2.5$	7000	3.08 ± 0.15	0.60 ± 0.03	0.35 ± 0.03	0.0483 ± 0.0250	0.0017 ± 0.0017	0.215
Figure 3(a)	LHCb	pp	$\mu\mu$, $2.5 < y < 3.0$	7000	3.02 ± 0.15	0.60 ± 0.03	0.35 ± 0.03	0.0476 ± 0.0250	0.0024 ± 0.0024	0.079
Figure 3(a)	LHCb	pp	$\mu\mu$, $3.0 < y < 3.5$	7000	2.91 ± 0.14	0.60 ± 0.03	0.35 ± 0.03	0.0589 ± 0.0300	0.0011 ± 0.0011	0.112
Figure 3(a)	LHCb	pp	$\mu\mu$, $3.5 < y < 4.0$	7000	2.82 ± 0.14	0.60 ± 0.03	0.34 ± 0.03	0.0600 ± 0.0300	—	0.136
Figure 3(a)	LHCb	pp	$\mu\mu$, $4.0 < y < 4.5$	7000	2.77 ± 0.14	0.60 ± 0.03	0.35 ± 0.03	0.0500 ± 0.0250	—	0.093
Figure 3(b)	PHENIX	pp	ee, $\lvert y\rvert < 0.35$	200	2.26 ± 0.11	0.64 ± 0.03	0.33 ± 0.03	0.030 ± 0.015	—	1.724
Figure 3(b)	PHENIX	pp	$\mu\mu$, $1.2 \leqslant \lvert y\rvert \leqslant 2.2$	200	2.17 ± 0.11	0.66 ± 0.03	0.30 ± 0.03	0.040 ± 0.020	—	3.011
Figure 4(a)	ALICE	Pb–Pb, 0%–20%	$\mu\mu$, $2.5 < y < 4$	2760	2.39 ± 0.12	0.60 ± 0.03	0.34 ± 0.03	0.057 ± 0.030	0.003 ± 0.003	0.325
Figure 4(a)	ALICE	Pb–Pb, 20%–40%	$\mu\mu$, $2.5 < y < 4$	2760	2.63 ± 0.14	0.63 ± 0.03	0.33 ± 0.03	0.036 ± 0.018	0.004 ± 0.004	1.257
Figure 4(a)	ALICE	Pb–Pb, 40%–90%	$\mu\mu$, $2.5 < y < 4$	2760	2.68 ± 0.13	0.60 ± 0.03	0.36 ± 0.03	0.026 ± 0.013	0.004 ± 0.004	1.861

Table 1. (Continued.)

Figures	Collaboration	Type	(Pseudo)rapidity	$\sqrt{s_{\mathrm{NN}}}$ (GeV)	κ_0	k_1	k_2	k_3	k_4	χ^2/ndf
Figure 4(b)	ALICE	Pb–Pb, 0%–20%	$\mu\mu$, $2.5 < y < 4$	5020	2.51 ± 0.12	0.59 ± 0.03	0.36 ± 0.03	0.041 ± 0.020	0.009 ± 0.004	0.202
Figure 4(c)	ALICE	Pb–Pb, 0%–20%	$\lvert y\rvert < 0.9$	5020	2.55 ± 0.13	0.57 ± 0.03	0.36 ± 0.03	0.060 ± 0.030	0.010 ± 0.010	5.233
Figure 4(c)	ALICE	Pb–Pb, 20%–40%	$\lvert y\rvert < 0.9$	5020	2.67 ± 0.14	0.57 ± 0.03	0.35 ± 0.03	0.060 ± 0.030	0.020 ± 0.020	1.142
Figure 4(c)	ALICE	Pb–Pb, 40%–90%	$\lvert y\rvert < 0.9$	5020	2.79 ± 0.14	0.60 ± 0.03	0.33 ± 0.03	0.046 ± 0.023	0.024 ± 0.012	8.472

Same as figure 1, figure 2 shows the transverse momentum spectra of inclusive J/ψ mesons produced in fixed target $p(\overline{p})$-nucleus, $\pi^{\pm}$-nucleus and central lead–lead (Pb–Pb) collisions at GeV energies, where σ and N on the vertical axis denote the cross-section and particle number, respectively. The corresponding decay channels, collision energies and collision types are marked in the panels. In figures 2(a) and (c), different powers of ten marked in the panels are used to scale the data for different collisions for clarity. The different symbols in panels 2(a)–(c) denote the experimental data measured by the HERA-B Collaboration [42] worked at the DESY corresponding to the rapidity interval $|y| \leqslant 1.185 \sim 1.345$, E789 Collaboration [43] worked at the FNAL corresponding to the pseudorapidity interval $|\eta| \leqslant 0.425$, NA50 Collaboration [44] worked at the CERN SPS corresponding to the rapidity interval $0 < y < 1$ [45], and E705 Collaboration [46] worked at the FNAL corresponding to the pseudorapidity interval $|\eta| \leqslant 1.040$ for $\pi^{\pm}$-nucleus interactions and $|\eta| \leqslant 2.008$ for $p(\overline{p})$-nucleus interactions. It should be noticed that the rapidity intervals in figure 2 are our calculated results in the center-of-mass reference frame. The vertical error bars given by the HERA-B, NA50 and E789 Collaborations denote the total uncertainties, while the vertical error bars given by the E705 Collaboration only denote the statistical uncertainties. The solid curves are our fitting results and the figure 2(d) express the same meaning as figure 1(d).

Some special cases are shown in figure 3. Figures 3(a) and (b) are, respectively, the transverse momentum spectra of inclusive J/ψ mesons produced in different collisions for special rapidity intervals. The corresponding rapidity intervals, collision energies, integrated luminosities and decay modes are marked in the panels. In figure 3(a), different powers of ten marked in the panel are used to scale the data measured in different rapidity intervals for clarity. The different symbols in panels 3(a)–(b) denote the experimental data measured by the (a) LHCb Collaboration [47] at the CERN LHC and (b) PHENIX Collaboration [52] at the BNL RHIC. The vertical error bars represent the total uncertainties, which combine the systematic and statistical uncertainties. The solid curves are our fitting results and the figure 3(c) express the same meaning as figure 1(d).

Same as figure 1, figure 4 shows the transverse momentum spectra of inclusive J/ψ mesons produced in Pb–Pb collisions at TeV energies, where σ and N on the vertical axis denote the cross-section and particle number, respectively. The corresponding collision energies, decay channels, rapidity intervals and centrality bin are marked in the panels. The different symbols in panels 4(a)–(c) denote the experimental data measured by the ALICE Collaboration at CERN LHC. The experimental data in panel 4(a) come from the [48] and the vertical error bars represent the total uncertainties which combine the systematic and statistical uncertainties. The experimental data in panel 4(b) come from the [49, 50]. The experimental data in panel 4(c) come from the [51], which are the preliminary results. The solid curves are our fitting results and the figure 4(d) express the same meaning as figure 1(d).

During the calculation process, we find that the string tensions for different components can be expressed in some regular patterns. For one collision, we just need one parameter related to the string tension, then we can get all the string tensions in different components. Assume that the parameter κ_0 is the coefficient related to the elementary string tension, then the value of the string tension for the jth component (κ_j) can be get through the following empirical formula

$$\kappa_j = \kappa_0^{j+1}, \tag{13}$$

which is observed by fitting the experimental data. In addition, the elementary string tension parameter (κ_0) exhibits an obvious dependence on the $\sqrt{s_{\rm NN}}$, which will be presented in figure 6.

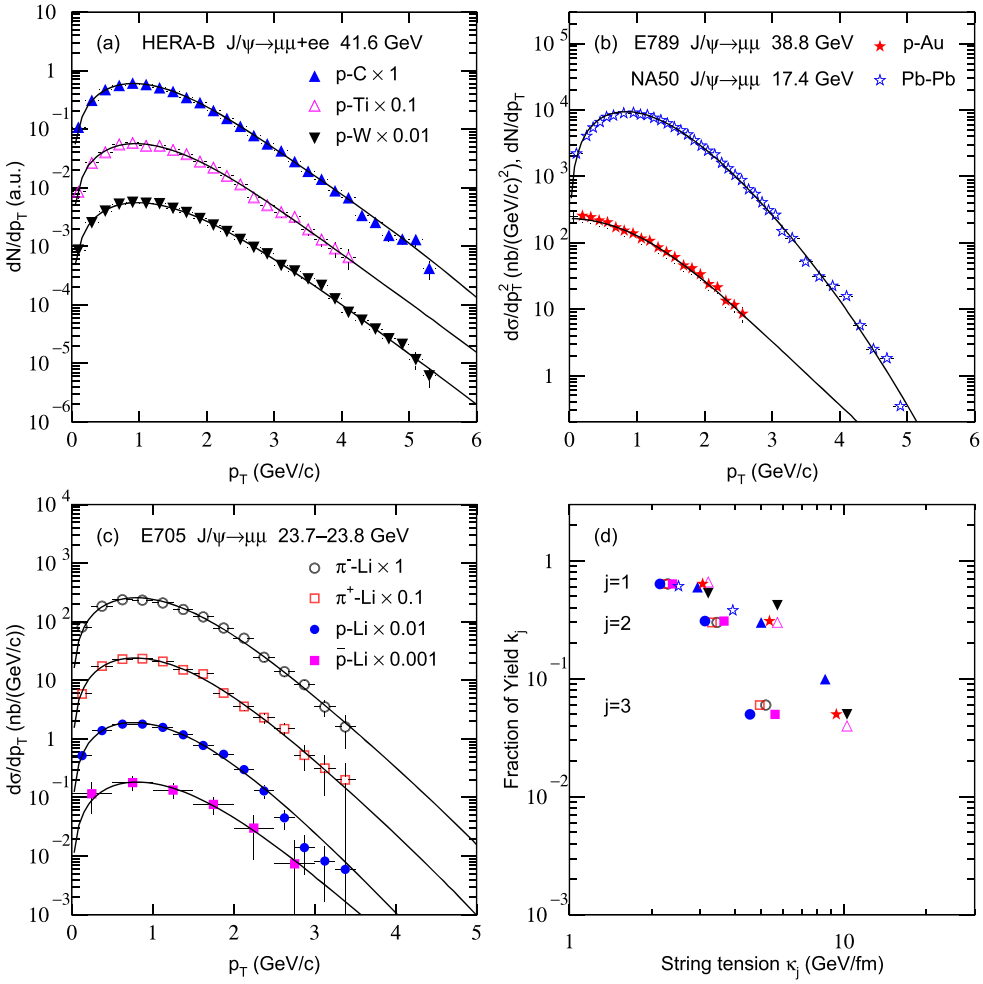

Figure 2. Same as figure 1, but showing the results of inclusive J/ψ mesons produced in the fixed-target collisions at GeV, where the collision types, decay modes and the center-of-mass energies are marked in the panels. The different symbols present the experimental data measured by the HERA-B [42], E789 [43], NA50 [44] and E705 [46] collaborations. The data for different collision types in panels (a) and (c) are scaled down by different powers of ten for clarity.

Based on equation (5) and the transverse momentum spectra of inclusive J/ψ mesons given by our model, the distributions of minimum distance between the partons which form the charmonium $c\bar{c}$ at different energies can be extracted. The results are shown in figure 5, and the corresponding center-of-mass energies, collision types and Collaborations are marked in the panels. The solid curves are the final results combined the relative contributions of all components. The dashed, dotted or dot-dashed curves from right to left presented in each panel are orderly the contributions of the first, second, third and fourth components. The minimum distance we extracted are mainly around 1 fm. It can be clearly observed that, with the increase of $\sqrt{s_{\rm NN}}$ over an energy range from 17.4 GeV to 13 TeV, the collision processes become more and more complicated, and there are more components presented in the

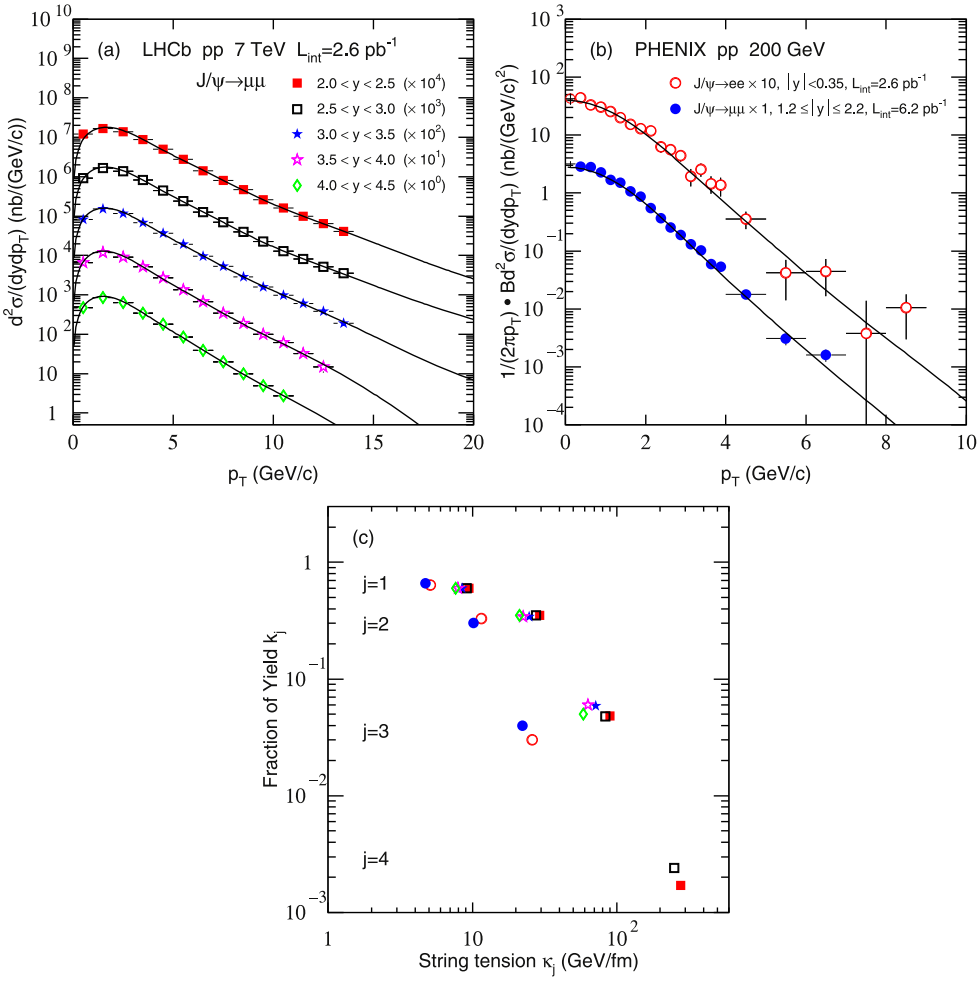

Figure 3. Same as figure 1, but showing the results of inclusive J/ψ mesons produced in different collisions, where the collision types, decays modes, rapidity intervals and the center-of-mass energies are marked in the panels. The different symbols represent the experimental data measured by the LHCb [47] and PHENIX [52] collaborations. The data in different rapidity intervals in panel (a) are scaled down by different powers of ten for clarity.

minimum distance distributions. At the same time, the distribution intervals for minimum distance between partons get narrower and narrower, the minimum as well as the maximum values of minimum distance get smaller and smaller. All the tendencies for the minimum distance between the partons which form the charmonium $c\bar{c}$ are the results of nature.

In order to reveal the tendencies of free parameters intuitively, figure 6 show the relations between (a) κ_0 and $\sqrt{s_{\rm NN}}$, (b) κ_0 and centrality bin, (c) κ_0 and y, and (d) the relative contribution for j and $\sqrt{s_{\rm NN}}$ in high energy collisions. From figure 6(a), one can see that the coefficient related to elementary string tensions show a linear dependence on the logarithm of $\sqrt{s_{\rm NN}}$. We give an empirical fit, and the result described by the solid curve is in the form as follows:

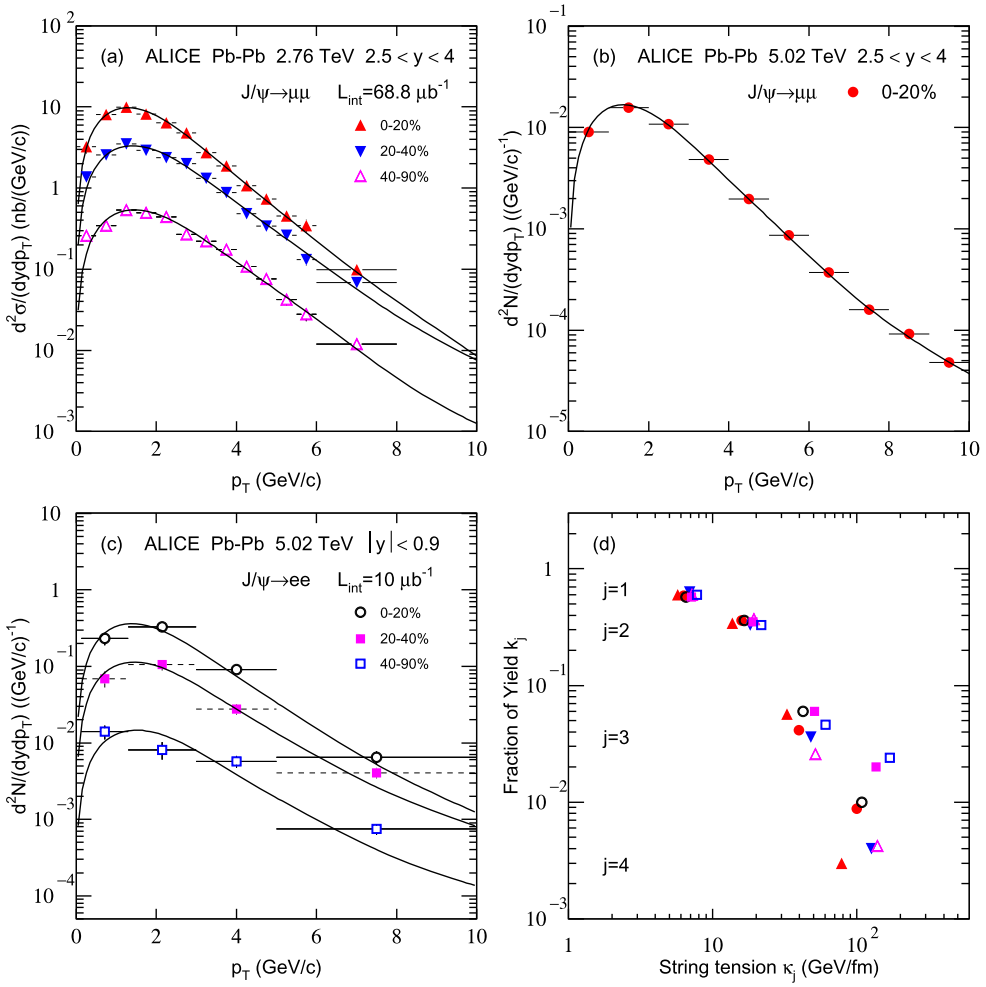

Figure 4. Same as figure 1, but showing the results of the inclusive J/ψ mesons produced in Pb–Pb collisions, where the centrality, decays modes, rapidity intervals and the center-of-mass energies are marked in the panels. The different symbols in panels (a)–(c) represent the experimental data measured by the ALICE [48–51] collaboration, and the different symbols in panel (c) represent the preliminary experimental data.

$$\kappa_0 = (0.236 \pm 0.015) \times \ln(\sqrt{s_{\rm NN}}) + (0.847 \pm 0.099). \tag{14}$$

Here, the fit of the black curve contains the results for particle–particle, particle–nucleus and nucleus–nucleus collisions, and the different type of the collisions will effect the prediction for special type collisions. What we want to emphasize is that we just give the tendency between the κ_0 and $\sqrt{s_{\rm NN}}$.

The increase of elementary string tension indicates the increase of color string field strength and partons energy. Considering the overlap and fuse of strings, the decrease of minimum distance between the binary partons we calculated indicates that one final state particle may contain more strings and more partons take part in the binary collisions. While a small amount of partons form a bound state, the large amount of partons form a new kind of

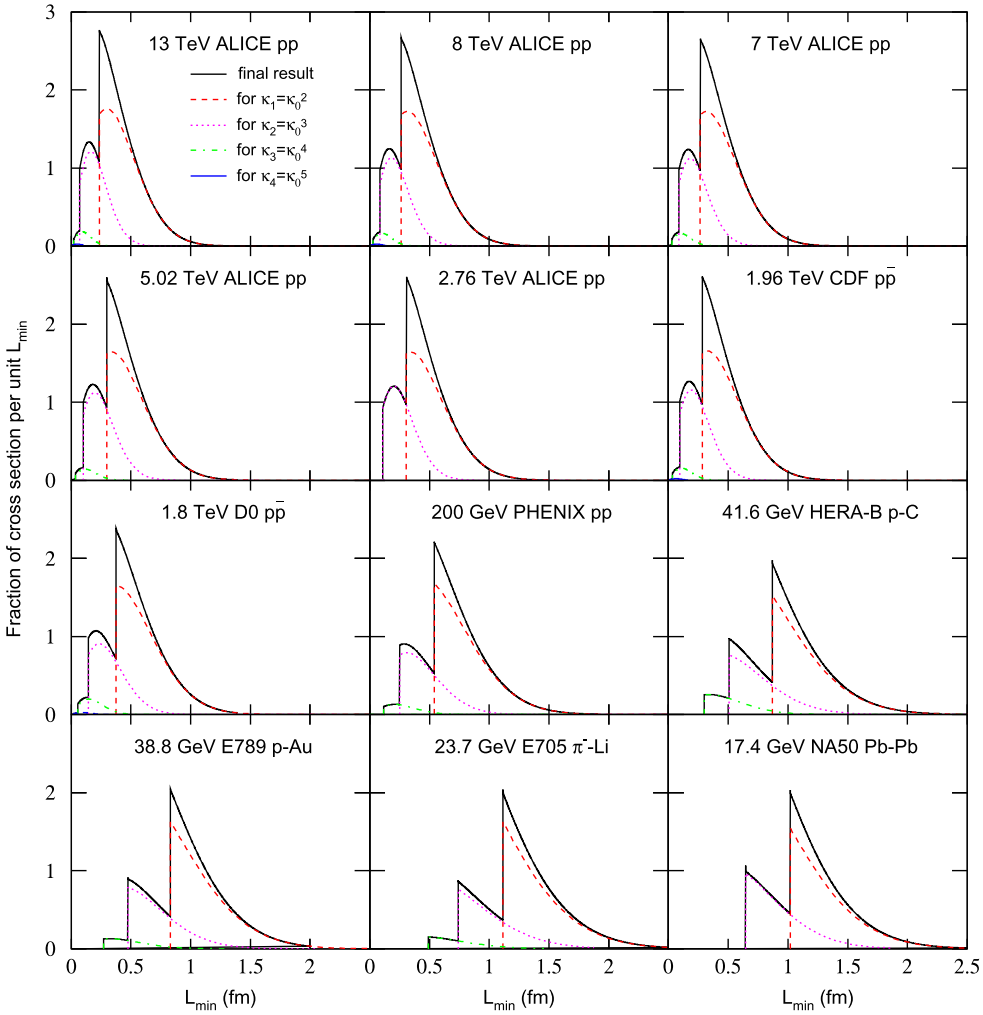

Figure 5. The minimum distance between the partons which form the J/ψ mesons in the collisions over an center-of-mass energy range from 17.4 GeV to 13 TeV.

matter, which is the QGP with more energy and higher density. This is consistent with the fact that if the collision energy is higher, the fireball created after the collision is hotter.

Figure 6(b) shows that the elementary string tension in peripheral Pb–Pb collisions are greater than those in central Pb–Pb collisions at 2.76 and 5.02 TeV. The elementary string tension increase obviously with the decrease of the centrality bin in nucleus–nucleus collisions. This phenomenon is mainly because some charm quarks will subjected to the effect of the QGP medium and lose energies when they cross the medium. In theory, the QGP medium will be formed in the center nucleus–nucleus collisions. Comparing with the center nucleus–nucleus collisions, less nucleons take part in the interactions and the $q\overline{q}$ produced in the hard scatters suffer less effect from the whole interactions in peripheral nucleus–nucleus collisions. Unfortunately, we can only judge the tendency of the elementary string tension changing with the centrality, but do not determine the type of the dependence due to the less amount of the data.

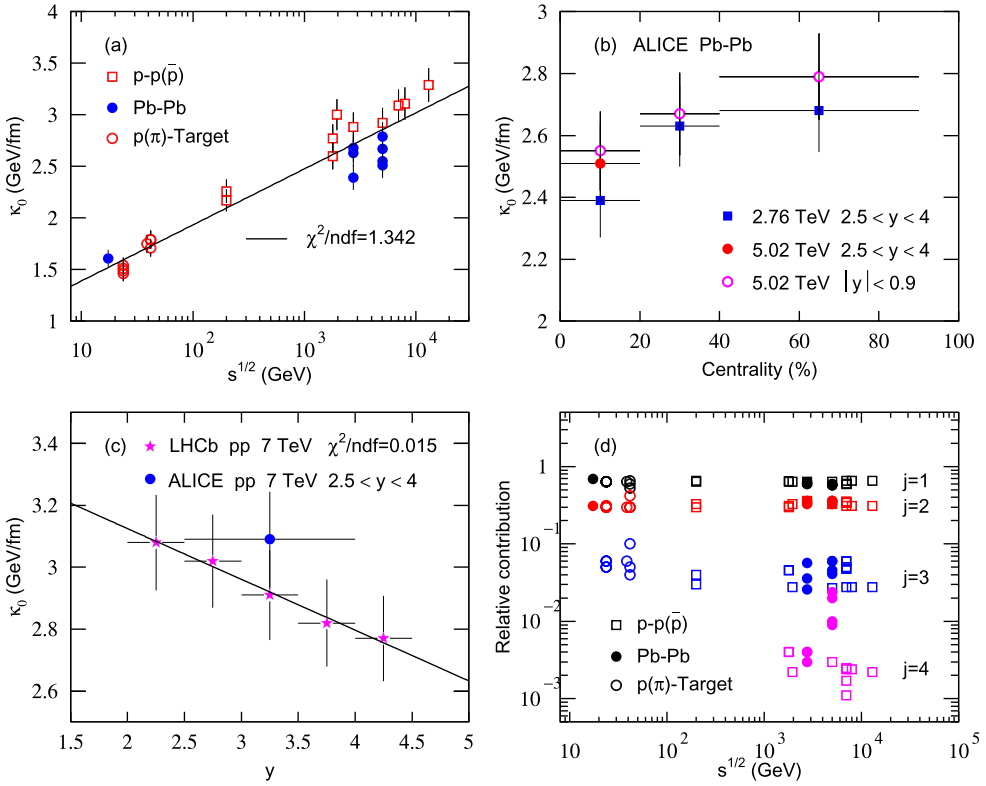

Figure 6. Relations between (a) κ_0 and $\sqrt{s_{\rm NN}}$, (b) κ_0 and centrality bin, (c) κ_0 and y, and (d) the relative contribution for j and $\sqrt{s_{\rm NN}}$ in high energy collisions. The different symbols present the values of parameters for the collisions measured at different conditions.

At the same time, we can see a clearly relation between the elementary string tension and rapidity in figure 6(c), which exhibits the results calculated from the *pp* collisions at 7 TeV with different rapidity intervals measured by the LHCb and ALICE Collaborations. We can see that the coefficient of the elementary string tension for the ALICE Collaborations is larger than that for the LHCb Collaborations. This is because the transverse momentum interval of the data measured by the ALICE Collaborations is larger than that measured by the LHCb Collaborations. The particles with bigger transverse momentum correspond to a larger string tension.

Due to the conversion of particle energy in the form of rapidity, the elementary string tension decreases with the increases of rapidity. Considering the particles with certain energies, particles produced in center rapidity region have higher transverse momentum than particles produced in forward rapidity region. So the elementary string tension extracted in forward rapidity region is smaller than that in central rapidity region. By comparing the calculation results, we find that the elementary string tension decreases with the increases of rapidity in a linear relation. Here we give an empirical fit in the following form

$$\kappa_0 = -(0.164 \pm 0.027) \times y + (3.453 \pm 0.043). \tag{15}$$

The relation between κ_0 and y can also be verified by the results of pp collision at 200 GeV, which is presented in figure 3(b) and table 1.

The relative contribution of different components for different kinds of collisions are shown in figure 6(d). The relative ratio of same components have similar values for different collisions over all the energies, which can be seen in table 1 and figures 1(b), 2(b) 3(c) and 4(d). The parameters k_j with similar values show the same trend changing with the transverse momentum domain. According to the relative contribution of each component, the productions of $q\bar{q}$ can be divided mainly into two kinds of processes. One is hard process corresponding to the first component, which accounts for more than 60% of the yield. Another is the harder process corresponding to the second component, which makes up more than thirty percent of the yield. There are only less than 5 % of the particles produced in the extremely violent collisions corresponding to others components. One major difference in the transverse momentum spectra for different energies is characterized by the shape of the tail, which is contributed by the components less than 5%. Generally, if the collision process is more violent, there are more energy transmitted to each other, the probability of the collision occurred is smaller. These results obey the nature regularities. At the same time, the number of the components also increases with the collision energy. We need three components to describe the transverse spectra at GeV energies, while at least four components at TeV energies.

The higher energy and density of partons will lead to more and more violent interactions between them, then the productions of the bound state $q\bar{q}$ can not be regarded as an equilibrium state. With the increases of the center-of-mass energy, the total energy of the system increases and the degree of non-equilibrium for the particle production also becomes larger and larger. This can be verified by the trend of the elementary string tension and the number of the components we used in the fit process. Due to the restriction of the experimental data, some special cases may not obey the law.

The values of the elementary string tension extracted in the present work are larger than the standard value of the string tension corresponding to the temperature $T = 170$ MeV [34], so the temperature of the binary parton system which produce the $q\bar{q}$ is higher than the 170 MeV. This result reconciles with the production of charmonium mainly in the hard partonic scatters of the initial stage. The minimum distance between the partons which form the observable particles is mainly around 1 fm, and this distance corresponds to the force which confined the quarks into hadrons in QCD [53].

4. Conclusions

We summarize our main observations and conclusions into the following three aspects.

(a) The transverse momentum spectra of inclusive J/ψ mesons produced in particle–particle, particle–nucleus and nucleus–nucleus collisions in a center-of-mass energy range from 17.4 GeV to 13 TeV can be analyzed by the multi-component Schwinger mechanism. The model results are well in agreement with the experimental data measured by the ALICE, CDF, D0, HERA-B, E789, NA50, E705, LHCb and PHENIX Collaborations. The value of the parameters related to string tension and relative ratio for different components are extracted.

(b) Based on the transverse momentum spectra of inclusive J/ψ mesons given by our model, the distribution of minimum distance between the partons which form the charmonium $c\bar{c}$ at different energies are extracted. The minimum distance between the partons extracted by us is mainly around 1 fm. With the increase of $\sqrt{s_{\rm NN}}$ over an energy range from

17.4 GeV to 13 TeV, the distribution intervals of minimum distance between partons get narrower and narrower, the minimum (as well as the maximum) value of the distribution interval also get smaller and smaller. Meanwhile, the collision processes become more and more complicated and there are more components presented in the minimum distance distribution.

(c) The parameter, coefficient of elementary string tension, is found to increase with the increase of energy and decrease with the increase of rapidity as well as centrality. The explicit relations between κ_0 and $\ln(\sqrt{s_{\rm NN}})$, κ_0 and rapidity can be fitted by special linear relation. At the same time, the relative contribution of same components have the similar values for different kinds of collisions.

Although our model is a simple model with a few parameters, which cannot explicitly include many different kinds of mechanisms about J/ψ productions, it can describe well transverse momentum spectra of J/ψ produced in particle–particle, particle–nucleus and central nucleus–nucleus collisions from 17.4 GeV to 13 TeV. We hope that the extracted parameters can provide some useful information about many aspects of J/ψ physics.

Acknowledgments

This work was supported by the National Natural Science Foundation of China under Grant Nos. 11947040, 11890710, 11835002, 11421505, and 11961131011, the Key Research Program of the Chinese Academy of Sciences under Grant No. XDPB09, and the Key Research Program of Frontier Sciences of the CAS under Grant No. QYZDJ-SSW-SLH002.

Conflict of interests

The authors declare that there is no conflict of interests regarding the publication of this paper.

ORCID iDs

Ya-Hui Chen https://orcid.org/0000-0002-4117-773X

References

[1] Munzinger P B and Stachel J 2007 *Nature* **448** 302
[2] Arsene I *et al* (BRAHMS Collaboration) 2005 *Nucl. Phys.* A **757** 1
[3] Back B B *et al* (PHOBOS Collaboration) 2005 *Nucl. Phys.* A **757** 28
[4] Adams J *et al* (STAR Collaboration) 2005 *Nucl. Phys.* A **757** 102
[5] Adcox K *et al* (PHENIX Collaboration) 2005 *Nucl. Phys.* A **757** 184
[6] Ludlam T 2005 *Nucl. Phys.* A **750** 9
[7] Chen J H *et al* 2018 *Phys. Rep.* **760** 1
[8] Chatrchyan S *et al* (CMS Collaboration) 2012 *Eur. Phys. J.* C **72** 1945
[9] Aamodt K *et al* (ALICE Collaboration) 2011 *Phys. Lett.* B **696** 30
[10] Andronic A *et al* 2018 *Nature* **561** 321
[11] Luo X and Xu N 2017 *Nucl. Sci. Tech.* **28** 112
[12] Zhang S H *et al* 2018 *Nucl. Sci. Tech.* **29** 136
[13] Lao H L *et al* 2018 *Nucl. Sci. Tech.* **29** 164
[14] Lao H L *et al* 2018 *Nucl. Sci. Tech.* **29** 82
[15] Mrowczynski S 2018 *Eur. Phys. J.* A **54** 43
[16] Song L H *et al* 2018 *Nucl. Sci. Tech.* **29** 159
[17] Prino F and Rapp R 2016 *J. Phys. G: Nucl. Part. Phys.* **43** 093002

[18] Wang H M *et al* 2018 *Nucl. Sci. Tech.* **29** 116
[19] Andronic A *et al* 2007 *Nucl. Phys.* A **789** 334
[20] Thews R L, Schroedter M and Rafelski J 2001 *Phys. Rev.* C **63** 054905
[21] Thews R L 2002 *Nucl. Phys.* A **702** 341
[22] Eichten E *et al* 1978 *Phys. Rev.* D **17** 3090
Eichten E *et al* 1980 *Phys. Rev.* D **21** 313 erratum
[23] Liu F H 2008 *Nucl. Phys.* A **810** 159
[24] Chen Y H, Liu F H and Lacey R A 2016 *Adv. High Energy Phys* **2016** 9876253
[25] Schwinger J S 1951 *Phys. Rev.* **82** 664
[26] Schwinger J S 1962 *Phys. Rev.* **128** 2425
[27] Casher A, Neuberger H and Nussinov S 1979 *Phys. Rev.* D **20** 179
[28] Glendenning N K and Matsui T 1983 *Phys. Rev.* D **28** 2890
[29] Andersson B *et al* 1983 *Phys. Rep.* **97** 31
[30] Adams J *et al* (STAR Collaboration) 2005 *Phys. Rev. Lett.* **94** 062301
[31] Matsui T and Satz H 1986 *Phys. Lett.* B **178** 416
[32] Liu Y P *et al* 2009 *Phys. Lett.* B **678** 72
[33] Armesto N, Pajares C and Sousa D 2002 *Phys. Lett.* B **527** 92
[34] Bialas A 1999 *Phys. Lett.* B **466** 301
[35] Gao L N and Liu F H 2016 *Adv. High Energy Phys* **2016** 1505823
[36] Wong C Y 1994 *Introduction to High-Energy Heavy Ion Collisions* (Singapore: World Scientific)
[37] Abelev B *et al* (ALICE Collaboration) 2012 *Phys. Lett.* B **718** 295
Abelev B *et al* (ALICE Collaboration) 2015 *Phys. Lett.* B **748** 472 erratum
[38] Acharya S *et al* (ALICE Collaboration) 2017 *Eur. Phys. J.* C **77** 392
[39] Acosta D *et al* (CDF Collaboration) 2005 *Phys. Rev.* D **71** 032001
[40] Abe F *et al* (CDF Collaboration) 1997 *Phys. Rev. Lett.* **79** 572
[41] Abbott B *et al* (D0 Collaboration) 1999 *Phys. Rev. Lett.* **82** 35
[42] Abt I *et al* (HERA-B Collaboration) 2009 *Eur. Phys. J.* C **60** 525
[43] Schub M H *et al* (E789 Collaboration) 1995 *Phys. Rev.* D **52** 1307
Schub M H *et al* (E789 Collaboration) 1996 *Phys. Rev.* D **53** 570 erratum
[44] Abreu M C *et al* (NA50 Collaboration) 2001 *Phys. Lett.* B **499** 85
[45] Abreu M C *et al* (NA50 Collaboration) 1997 *Phys. Lett.* B **410** 327
[46] Antoniazzi L *et al* (E705 Collaboration) 1992 *Phys. Rev.* D **46** 4828
[47] Aaij R *et al* (LHCb Collaboration) 2011 *Eur. Phys. J.* C **71** 1645
[48] Adam J *et al* (ALICE Collaboration) 2016 *J. High Energy Phys.* JHEP05(2016)179
[49] Adam J *et al* (ALICE Collaboration) 2017 *Phys. Lett.* B **766** 212
[50] Andronic A *et al* 2019 *Phys. Lett.* B **797** 134836
[51] Acharya S *et al* (ALICE Collaboration) arXiv:1910.14404 [nucl-ex]
[52] Adare A *et al* (PHENIX Collaboration) 2007 *Phys. Rev. Lett.* **98** 232002
[53] Nouicer R 2016 *Eur. Phys. J. Plus* **131** 70